QUANTITATIVE ASSESSMENT OF PORE DEVELOPMENT AT Al_2O_3/FeAl INTERFACES DURING HIGH TEMPERATURE OXIDATION

P. Y. Hou, C. Van Lienden, Y. Niu[*] and F. Gesmundo[+]

Materials Sciences Division
Lawrence Berkeley National Laboratory
Berkeley, CA 94720

*Chinese Academy of Sciences
Institute of Metals Research
Shenyang, P. R. China

+Istituto di Chimica
Universita di Genova
16129 Genova, Italy

ABSTRACT

Alloys of commercial grades that do not contain a reactive element, such as yttrium, often develop pores at the scale/alloy interface. The accumulation and growth of these pores greatly weaken scale adhesion. The purpose of this study is to evaluate pore development in Fe-40at%Al and determine the change in pore volume with oxidation time. Experimental results are then compared to a theoretical calculation where all vacancies are allowed to condense as voids. After removing the oxide scales that formed after various times of oxidation at 1000°C in oxygen, the alloy surface was analyzed using scanning electron microscopy (SEM) and atomic force microscopy (AFM) to determine the size and depth of interfacial pores. Results are discussed in light of possible mechanisms involved in pore formation at scale/alloy interfaces.

INTRODUCTION

One common result in high temperature corrosion, where a surface scale develops on the substrate under oxidizing environments, is the presence of pores in the scale, at the scale/alloy interface and/or within the substrate. When their size and/or density reach a critical value, they can severely deteriorate the mechanical property of the medium in which they are present. For Al_2O_3 scales formed on commercial grade alloys without any reactive elements, such as yttrium, pores are commonly found in the scale or at the scale/alloy interface (1). These alloys usually contain 10-20 ppm sulfur as a common impurity, and its presence is believed to stabilize interfacial pores (2).

The mechanism of pore formation was first suggested to be that of vacancy condensation (3), where cation vacancies from the scale injecting to the scale/alloy interface condense to form voids. Whether this is indeed the case is uncertain. There is also very little knowledge of its

relevance with different scale/alloy systems. Others have proposed oxide growth stresses (4) and uneven diffusional flux of alloying elements (5) as alternative causes. It is our view that the development of voids will have to be quantified first before understanding of their nucleation and growth processes can be attained. Phenomenological studies alone of the appearance and morphology of pores are not sufficient. Hence, this study attempts to characterize pore size and volume as a function of oxidation time, then compare the experimentally determined volume with theoretical calculation where all vacancies are allowed to condense as voids.

Fe-40at%Al was chosen because it forms pronounced interfacial pores (6,7,8). The alloy is single phased with a CsCl structure. Its structure and oxidation behavior are similar to that of β-NiAl, where transition θ or γ-Al_2O_3 forms first, then α-Al_2O_3 nucleates at the scale/alloy interface; the initially formed Al_2O_3 eventually transforms to α with time. The transition Al_2O_3 grows predominantly by aluminum outward transport and the α-Al_2O_3 predominantly by oxygen inward transport. The growth rate of the former is about one order of magnitude faster than the latter (6,9,10).

The amount of interfacial voids on FeAl seemed to increase with alloy aluminum content, from 10-48 at%, while the oxidation rate remained unchanged (6). Interfacial void concentration on Ni-(40-55at%)Al was found to be higher on the Ni-rich materials, where Ni in the alloy was expected to diffuse much faster than Al (11). In that study, the mechanism of void formation was attributed to the Kirkendall effect where the different Ni and Al diffusion rates caused a net flux of vacancy to the scale/alloy interface. Xu et al (7) noted that most interfacial pores formed at the Al_2O_3/FeAl interfaces were faceted with distinct crystallographic orientation. This led them to suggest that pores formed as a result of Al vapor transport.

EXPERIMENTAL

The FeAl alloy, from Oak Ridge National Laboratory, was prepared by arc melting and casting, followed by hot rolling to a ~ 1 mm thick sheet. The alloy contains 40at% aluminum and 27.6 ppm of sulfur impurity. Specimens typically 15mm x 10 mm x 1mm were cut from the sheet and polished to a 1 μm finish with diamond paste and cleaned ultrasonically in acetone. One specimen was wrapped in tantalum and heated under argon at 1000°C for 5 hours, then furnace cooled to evaluate the effect of heat treatment on pore formation. All other specimens were oxidized in flowing, dry oxygen at 1000°C. A Cahn TGA system was used for thermogravemetic analysis. Other specimens were placed in an alumina boat with a thermocouple at its back and oxidized in a horizontal furnace. After the desired oxidation time, which varied from 3 min to 24 hours, the boat and specimen were quickly pulled out of the furnace and cooled in ambient air. In both systems, the specimen temperature took about 10 minutes to stabilize at 1000°C.

The scale on samples oxidized for longer than 1 hour spalled during cooling. Delaminated oxide pieces were removed by ultrasonic vibration to expose the underlying metal surfaces for further examination. Portions of scales that did not spall during cooling were removed by first gluing a 3 mm round aluminum post to the sample surface then striped off when the post was

knocked away. The scale/alloy interface on the 3 and 10-minute samples was too strong for the oxide to be removed this way. Alloy surfaces in these cases were exposed by the motion of deep, several millimeter long scratches that were made with a diamond stylus on the specimen surface [8]. This caused extensive scale delamination and spallation around the scratches.

Compositions of very thin scales were determined using Auger depth profiling. Structure of the scale was studied using X-ray diffraction and the morphology examined using Scanning electron microscopy (SEM). A few specimens were mounted and cross-sectioned to investigate the amount of porosity in the alloy, if any.

Quantification of interfacial pores was made by analyzing SEM micrographs of the alloy surface. Some of the specimens were also studied using atomic force microscopy (AFM) to determine the depth of these pores. SEM images of areas where the scale had been removed were taken in a random manner across the specimen, covering several different alloy grains. The perimeter of each pore on a given SEM micrograph was first traced, then the pore area on the scale/alloy interface was determined using an image analysis software. To locate pores using the AFM, initial 80x80 or 100x100 μm scans were made on the specimen surface. Locations were randomly chosen but spaced wide enough to cover different alloy grains. Smaller images (usually less than 20x20 μm) were subsequently taken over single or multiple pores until all the pores in the larger scan were analyzed. Two line scans were made on each pore, one horizontal and one vertical, crossing at the center of the pore, to determine the pore depth and diameter. All the scans were made with ultra-sharp contact silicon cantilevers, which have a cone angle of $<20^{o}$.

RESULTS AND DISCUSSIONS

Oxidation Kinetics

Specimen weight gain as a function of time$^{1/2}$ is plotted in Figure 1 to evaluate the oxidation kinetics. The rate was significantly faster during the first hour, followed by a gradual decrease until a slower constant is reached. The rate constants for the two stages were $1x10^{-12}$ and $4.4x10^{-14}$ $g^2cm^{-4}s^{-1}$ respectively, which compare well with previously reported rates on FeAl [6,9] and NiAl [10]. XRD studies showed evidence of θ-Al_2O_3 during the early stages of oxidation, but α-Al_2O_3 dominated after 1 hour.

Scale and Interface Microstructure

Morphologies of oxide scale and the alloy surface after different oxidation times are shown in Figure 2. The thinnest scale studied was oxidized for only 3 minutes (Fig. 2a). Auger depth profile found this scale to be a single layer of Al_2O_3. Very fine and uniform grains, ~ 50 nm in diameter, existed on the outer surface, yet pores about 0.5 μm were observed on the alloy surface. Facetted α-Al_2O_3 grains started to nucleate at the scale/alloy interface after 10 minutes. A complete layer of α-Al_2O_3 developed after 1 hour. The average oxide grain size at the interface after this time stayed fairly constant and was about 0.3 μm, but interfacial pores were often larger than 1 μm (Fig. 2b). Pores developed randomly throughout the entire interface.

Preferential formation was only found along polishing marks on the original surface, but not on alloy grain boundaries and there was no obvious variation from different alloy grains. Groups of pores were occasional observed that probably resulted from surface contamination prior to oxidation. Nearby pores sometimes jointed together into larger ones, an example is given in Fig. 2d. Whenever it was possible to distinguish those that were undergoing coalescence, they were counted as separate individual pores.

All the pores being analyzed in this work were about an order of magnitude larger than the oxide grain size. They often contain discrete crystallographic planes on their sides and bottoms, especially on larger ones. This gave the pores a characteristic shape that depended on the alloy grain (Fig. 2c). Sulfur was found present on the metal side of all pores (8). This coverage is expected to reduce the interface energy of the alloy (12) and thus stabilize the pores. The equilibrium shape must then be one that minimizes the total surface energy while keeping the force balance at the pore/interface junction to satisfy $\gamma_{interface} = \gamma_{oxide} + \cos\theta\, \gamma_{metal}$, where θ is the angle between the pore and the interface, and the γ's are the interfacial energies.

It is important to note that pore formation was not observed when the specimen was heat-treated without oxidation. Pores were also not observed within the alloy beneath the scale. This shows that all pores were contained at the scale/alloy interface and their formation is only a result of the oxidation process, not the condensation of excess thermal vacancies from the alloy (13). The portion of scale above pores was similar in thickness and morphology with that on the rest of the specimen surface (14,15). This suggests that scale growth above pores was unaffected by their presence.

Quantitative Analysis of Interfacial Pores

AFM was used to measure pore depth as a function of pore size and oxidation time. Two orthogonal line traces were made across each pore center to determine its depth, width and length. Depth was identified as the distance between the deepest point into the alloy from the alloy surface. Width and length were taken from the line distance across the pore face that is in the plane of the scale/alloy interface. Summary of the data collected from every pore that was mapped using AFM is given in Figure 3, where the depth of each pore is plotted against the average of its width and length. The average aspect ratio was calculated to be 1.22 ± 0.2, which shows that most of the pores have a near circular face despite their highly facetted sides and bottoms. Although the data in Fig. 3 scattered, they show an overall linear relationship between pore diameter and depth. This means larger pores were also deeper, so pore growth must involve extension along the interface as well as into the alloy regardless of the pore shape. Most of the data can be fitted with a slope of about 0.2 and some, mainly those from 24 hrs, with a slope of 0.1. These numbers show that the first-formed pores were shallow, having an average diameter, *d*, 5 times larger than the depth. With increased oxidation time, the pores increased in diameter as well as in depth, keeping the *d/h* ratio fairly constant until coalescence of nearby pores took place. As two pores of similar depth grew into one, the *d/h* ratio then increased to about 10.

To evaluate the rate of pore growth, the average pore diameter obtained from SEM analysis and depth from AFM are plotted against the square root of time in Figure 4. Pores are again seen to be about 5 times bigger in diameter than in depth, confirming the AFM results presented in Figure 3. The increase in the average *d* and *h* with time is seen to be near parabolic with a faster rate within the first hour and a 5-6 times slower steady state rate afterwards. The behavior is similar to the scale weight gain results, where the initial rate was faster than the steady state rate, which was established after about 3 hours. Microstructural observations showed that the steady state behavior corresponded to the formation of a complete α-Al_2O_3 that nucleated at the scale/alloy interface.

From Figure 4, the steady state pore growth rate can be calculated to be 1.8×10^{-7} moles of Al per cm^2 of pore surface per hour, using volume = $\frac{1}{2}\pi(d/2)^2h$. The oxide growth rate requires 1.3×10^{-7} moles(Al)/cm^2h. The closeness of these two numbers suggests that pore enlargement under steady state scaling condition resulted from Al vapor transport to support continued scale growth above the pores. The vapor pressure of Al in equilibrium with the surface of the Fe-40Al alloy under an Al_2O_3 scale was calculated [16] to be 4.65×10^{-9} atm at 1000°C, which is more than 3 orders of magnitude higher than the equilibrium pO_2 level, hence giving sufficient Al supply for scale growth. The excellent agreement between the pore and scale growth rates may be coincidental due to uncertainties in the pore growth rate calculation. A large scatter of pore sizes actually existed and the pore geometry was approximated. For longer oxidation times, size increase would also have resulted from pore coalescence rather than pore growth. However, these uncertainties combined should still give an order of magnitude agreement with the scale growth data.

Analysis of Vacancy Content from Oxidation

Details of this analysis are given elsewhere (16). Basically, two vacancy fluxes are considered: one is that due to oxide growth, J_V^{ox}, the other is from an unbalanced diffusion of Fe and Al in the alloy, i.e. from the Kirkendall effect, J_V^K. Diffusion coefficients of Fe and Al are assumed to be independent of composition. No vacancy annihilation is allowed anywhere, and lattice volume is conserved whereas relaxation due to vacancy formation is not considered. The flux associated with oxide growth is first analyzed for the case of exclusive cation diffusion, then a fraction that changes with time is introduced to account for the degree of growth due to anion diffusion. For every cation that is transported through the scale, an equivalent volume of vacancy is allowed to condense at the scale/alloy interface. Anion transport does not contribute to the total vacancy content, since vacancies in that case are eliminated at the outer scale surface.

The total weight gain from scale growth per unit surface area after time t, $\Delta m/A$, is related to the total amount of Al incorporated into the scale from the alloy. The overall rate of Al supply to the scale, J_{Al}^{ov}, has two components. One is the flux of Al diffusing from the alloy to the alloy/scale interface, J_{Al}. The other is the rate of Al incorporation due to the inward displacement with time of the alloy/scale interface, J'_{Al}. Therefore we have

$$J_{Al}^{ov} = J_{Al} + J'_{Al} = - [d(\Delta m/A)/dt]/(3M_O/2) \quad (1)$$

where M_O is the atomic weight of oxygen. In turn, J'_{Al} is given by

$$J'_{Al} = - c^\circ N_{Al}^{i} \, dh/dt = - N_{Al}^{i} [d(\Delta m/A)/dt]/(3 M_O/2) \quad (2)$$

where c^0 is the overall concentration of metal in the alloy in mol/cm^3, N_{Al}^{i} the mole fraction of Al at the scale/alloy interface and h the thickness of metal consumed due to oxidation.

The flux of Al diffusing from the alloy to the scale/alloy interface, J_{Al}, can be determined by combining Eqns. (1) and (2). The flux of Fe in the opposite direction is related to J_{Al} by the relation $J_{Fe} = - J_{Al} D_{Fe}/D_{Al}$, where the D's are the diffusion coefficients. Finally, the overall flux of metal vacancies at the alloy/scale interface due to diffusion in the alloy, J_V^K, is simply opposite to the sum of the two metal fluxes, which yields

$$J_V^K = (1 - N_{Al}^{i}) (1 - D_{Fe}/D_{Al}) [d(\Delta m/A)/dt]/(3M_O/2) \quad (3)$$

In case of exclusive cation diffusion in the scale, the flux of aluminum through the scale, J_{Al}^{ox}, is equal to the overall flux of Al crossing the alloy/scale interface, J_{Al}^{ov}. In this situation, the flux of metal vacancies reaching the alloy/scale interface due to transport through the scale, J_V^{ox}, is equal and opposite to the flux of metal crossing the alloy/scale interface, J_{Al}^{ov}, and is thus given by Eq.(1) with a change in sign. Finally, the rate of accumulation of metal vacancies at the alloy/scale interface is given by the difference between J_V^{ox} and J_V^K, ΔJ_V, yielding

$$\Delta J_V = [d (\Delta m/A)/dt][(D_{Fe}/D_{Al} + N_{Al}^{i} (1 - D_{Fe}/D_{Al})]/(3M_O/2) \quad (4a)$$

In case of mixed cation-anion conduction, the flux of vacancies due to oxide growth is modified as $J_V^{ox} = - \lambda J_{Al}^{ov}$, where λ is the fraction of cation transport. Combination of the two vacancy contributions from the scale and the alloy, while taking into account λ, yields the net rate of vacancy accumulation from the oxidation process as

$$\Delta J_V = [d (\Delta m/A)/dt][(D_{Fe}/D_{Al} - (1- \lambda) + N_{Al}^{i} (1 - D_{Fe}/D_{Al})]/(3M_O/2) \quad (4b)$$

Eq.(4b) can be used to calculate the total vacancy content knowing the oxidation weight gain, diffusivities of Fe and Al in the alloy, concentration of Al at the scale/alloy interface and the factor λ, which can be approximated from the transport properties through alumina scales.

α-Al_2O_3 scales are known to grow predominately by oxygen inward diffusion (17-19), and the fraction of cation transport through an α-Al_2O_3 layer is estimated from limited oxygen isotope studies to be about 0.2 (19). After a complete α layer forms on FeAl, transport through the scale should be dominated by it and λ, the fraction of cation diffusion, was given a value of 0.2. During the initial oxidation stage, transition alumina grew on the specimen surface, where cation diffusion dominates (17), λ at this time was accordingly taken to be 0.8. The change of λ with time from its maximum to minimum values depends on when and how the α layer forms. The exact time dependence of this process is not known. Base on the experimental results that α grains started to be observed at the scale/alloy interface after 10 min and a complete layer established at 1hr, the time dependence was simulated by means of a sigmoidal function σ of the

type $\sigma = 1 - \exp[-5\ t^4]$, where t is the oxidation time in hours. If λ is assumed to be simply proportional to σ, it is given by the equation $\lambda = \lambda_{min} + (\lambda_{max} - \lambda_{min})\ \sigma$. These functions are plotted in Fig. 5a with λ_{min}=0.2, λ_{max}=0.8 and t_{crit} (the time needed to reach σ very close to unity) equals 1 hr.

The diffusion coefficients of iron and aluminum in the alloys have been measured recently for iron, while accurate measurements for Al are not possible due to the lack of a radioactive Al isotope with a half-life of convenient duration. Therefore, an isotope of In has been used to make diffusion measurements in Fe-Al alloys, assuming that its diffusion coefficient may be relatively close to that of Al. For an alloy composition corresponding to FeAl, the diffusion coefficients are given by (20,21)

$$D_{Fe}\ (cm^2s^{-1}) = 53\ \exp(-265\ kJ/mol\ /RT)\ ,\ D_{In}\ (cm^2s^{-1}) = 64\ \exp(-258\ kJ/mol\ /RT)$$

Using these diffusivities and the oxidation kinetics, the total amount of vacancies from the scale and the alloy and their difference is calculated and shown in Fig. 5b. Vacancy contribution from the Kirkendall effect is only affected by the oxidation rate, not by phase transformation of the alumina scale. Since Al diffuses faster than Fe in the alloy, the transport of Al to the interface to form oxide results in a flux of vacancies away from the scale/alloy interface. Vacancies from the scale, on the other hand, depend on the alumina phase transformation, hence the choice of the λ and σ functions. The difference between the two fluxes undergoes a maximum before 1hr and then decreases slowly. The maximum arises because initial scale growth was dominated by cation transport that provided a flux of vacancies from the scale to the scale/alloy interface. After α-Al_2O_3 fully establishes in the scale, vacancy supply from the oxide is reduced and the difference in the two fluxes becomes approximately constant, i.e. vacancies stop to accumulate at the interface. Changing the λ and σ functions affects the final vacancy content and time dependence: in particular, if tcrit is increased the maximum tends to disappear, but the effects are small and the overall time dependence remains the same.

Mechanism of Pore Growth

Experimentally determined pore volume per unit area as a function of oxidation time is shown in Figure 6. Pore area for each sample was determined from SEM analysis by adding the areas of all observed pores and comparing that to the total interface area examined. Pore depths were obtained from the best fit of the AFM results shown in Fig. 4. Volume was again calculated using $\frac{1}{2}\pi d^2 h$. The error bars were those from the area analysis. All data points showed large scatters, because pores were very randomly distributed and a wide range of sizes existed on each sample. The trend shows that pore formation was most rapid during the initial stage, it then increased slowly and finally began to decrease after prolonged oxidation. This decrease is partly due to coalescence of neighboring pores, and partly due to new growth of oxide within larger pores, probably as a result of oxygen penetration from the scale. The magnitude of the pore volume is seen to be about 20 times lower than the calculated total vacancy content. Although there is a large error bar associated with the data and calculations were made with some assumptions on pore geometry, the data can be trusted within an order of magnitude. The

discrepancy between theory and experiment suggests that not all vacancies condensed into voids and annihilation processes must have taken place. Another interesting comparison is the change of pore and total vacancy volumes with time. The calculation shows that after about 1 hr, the total vacancy content remains constant, or decreases slightly due to faster diffusion of Al than Fe in the alloy. The experimental data, on the other hand, showed significant volume increase up to 3 hrs, followed by a slower increase to 5hr. This suggests that vacancy condensation may be responsible for pore nucleation, but not its growth.

The pore growth process observed in this work suggests that, at steady stage, aluminum evaporation is the responsible mechanism. There are three reasons for this conclusion. First, growth of the scales above the pores are not affected, so there must be a continuous and uniform Al supply to the oxide above the void face. This supply is available, since relatively high aluminum vapor pressure exists within the pores. Second, there was uniform growth of pore diameter and depth with time in a parabolic fashion that is similar to the scale growth rate. This suggests that materials were removed from all of the pore surfaces to support scale growth above the pores. Third, the pores developed into characteristic shapes in relation to the underlying alloy grains. These shapes must be a result of minimizing the surface energy while keeping an energy balance at pore edges. Evaporation causes uniform depletion of Al from the pore surfaces, which would be able to maintain this equilibrium shape. Non-uniform stress distribution along the pore and around the alloy surrounding it is known to exist (22,23), which can cause pore enlargement. According to the analysis of Wright et al (23) on a football shaped pore at Al_2O_3/Fe_3Al interface, enlargement in pore area can occur if tensile stresses at the pore edge exceed the interface strength. This process involves creation of new surfaces and perturbs the equilibrium pore shape, which should be energetically less favorable. The effect of stresses on pore growth may be more important during the initial stage before an equilibrium shape is established.

CONCLUSIONS

Quantitative assessment of pore growth at Al_2O_3/FeAl interface after 3 min - 24 hr oxidation have revealed several characteristics of these pores. They develop as a result of oxidation from the very early stages. An equilibrium shape is reached that depends on alloy grains. The pore diameter is about 10 times larger than the oxide grain size. Pores are shallow, with its wide/depth ratio ~5, and showing specific crystallographic planes on their faces. Growth of the pores involves widening as well as deepening. The growth rate is parabolic with a fast initial rate and a slow steady state rate. Scale growth above the pores is unaffected, and steady state pore growth is shown to be a result of aluminum vapor transport. Vacancies arriving at the scale/alloy interface as a result of scale growth by cation transport may be responsible for pore nucleation, but not their continued growth.

ACKNOWLEDGMENT

Research sponsored by the U. S. Department of Energy under contract No. DE-AC03-76SF00098.

REFERENCES

1. B. Pint, "On the formation of interfacial and internal voids in α-Al_2O_3 scales," *Oxid. Met.*, **48**, 303 (1997).

2. H. J. Grabke, D. Wiemer and H. Viefhaus, "Segregation of sulfur during growth of oxide scales", *Appl. Surf. Sci.*, **47**, 243 (1991).

3. A. Dravnieks and H. J. McDonald, *J. Electrochem. Soc.*, **94**, 139 (1948).

4. J. E. Harris, "Vacancy injection during oxidation: a re-examination of the evidence," *Acta Metall.*, **26**, 1033 (1978).

5. A. Kumar, M. Nasrallah and D. L. Douglass, , "Effect of Yt and Th on the oxidation behavior of Ni-Cr-Al alloys," *Oxid. Met.*, **8**, 227 (1974).

6. J. L. Smialek, J. Doychak and D. J. Gaydosh, "Oxidation behavior of FeAl+Hf, Zr, B," *Oxid. Met.*, **34**, 259 (1990).

7. C. H. Xu, W. Gao and H. Gong, "Oxidation behavior of FeAl intermetallics - the formation of pit-like holes on the substrate," *High Temp. Mater. and Proc.*, **19**, 371 (2000).

8. P. Y. Hou, "Impurity segregation to scale/alloy interfaces and its effect on interfacial properties," to be published in *Materials Science Forum*.

9. I. Rommerskirchen, B. Eltester and H. J. Grabke, "Oxidation of β-FeAl and Fe-Al alloys," *Mater. and Corr.*, **47**, 646 (1996).

10. M. W. Brumm and H. J. Grabke, "The oxidation behaviour of NiAl. I. Phase transformations in the alumina scale during oxidation of NiAl and NiAl-Cr alloys," *Corr. Sci.*, **33**, 1677 (1992).

11. M. W. Brumm and H. J. Grabke, "Oxidation behavior of NiAl--II. Cavity formation beneath the oxide scale on NiAl of different stoichiometries," *Corr. Sci.*, **34**, 547 (1993).

12. F. A. Halden and W. D. Kingery, *J. Phys. Chem.*, **59**, 557 (1955).

13. Y. A. Chang, L. M. Pike, C. T. Liu, A. R. Bilbrey and D. S. Stone, "Correlation of the hardness and vacancy concentration in FeAl," *Intermetallics*, **1**, 107 (1993).

14. R. Hutchings, M. H. Loretto and R. E. Smallman, "Oxidation of intermetallic compound NiAl", *Metal Sci.*, **15**, 7 (1981).

15. P. Y. Hou, Y. Niu and C. Van Lienden, "Analysis of pore formation at oxide/alloy interfaces, part I. Experimental results on FeAl", paper submitted to *Oxid. Met.*

16. F. Gesmundo and P. Y. Hou, "Analysis of pore formation at oxide/alloy interfaces, part II. Theoretical treatment of vacancy condensation," paper submitted to *Oxid. Met.*

17. K. P. R. Reddy, J. L. Smialek and A. R. Cooper, "Oxygen-18 tracer studies of Al_2O_3 scale formation on NiCrAl alloys," *Oxid. Met*., **17**, 429 (1982).

18. J. Jedlinski, and G. Borchardt, "On the oxidation mechanism of alumina formers," *Oxid. Met*., **36**, 317 (1991).

19 E. Schumann, J. C. Yang, M. Ruhle and M. J. Graham, "The effect of yttrium and zirconium on the oxidation of NiAl," *Mater. and Corr*., **47**, 631 (1996).

20. H. Mehrer, N. Eggersmann, A. Gude, M. Salamon and B. Sepiol, "Diffusion in intermetallic phases of the Fe-Al and Fe-Si systems," *Mat. Sci. Eng*., **A239-240**, 889 (1997).

21. H. Mehrer, "Diffusion in Intermetallics," *Mater. Trans. JIM (Japan)*, **37**, 1259 (1996).

22. A. G. Evans, G. B. Crumley and R. E. Demaray, "On the mechanical behavior of brittle coatings and layers," *Oxid. Metals*, **20**, 193 (1983).

23. J. K. Wright, R. L. Williamson, P. Y. Hou, R. M. Cannon, D. Renusch, B. Veal and M. Grimsditch, "Finite element modeling of the effect of interface anomalies on thermal stresses in alumina scales," in *High Temperature Corrosion and Materials Chemistry*, ed. P. Y. Hou, M. J. McNallan, R. Oltra, E. J. Opila and D. A. Shores, pp. 53-61, the Electrochem. Soc., 1998.

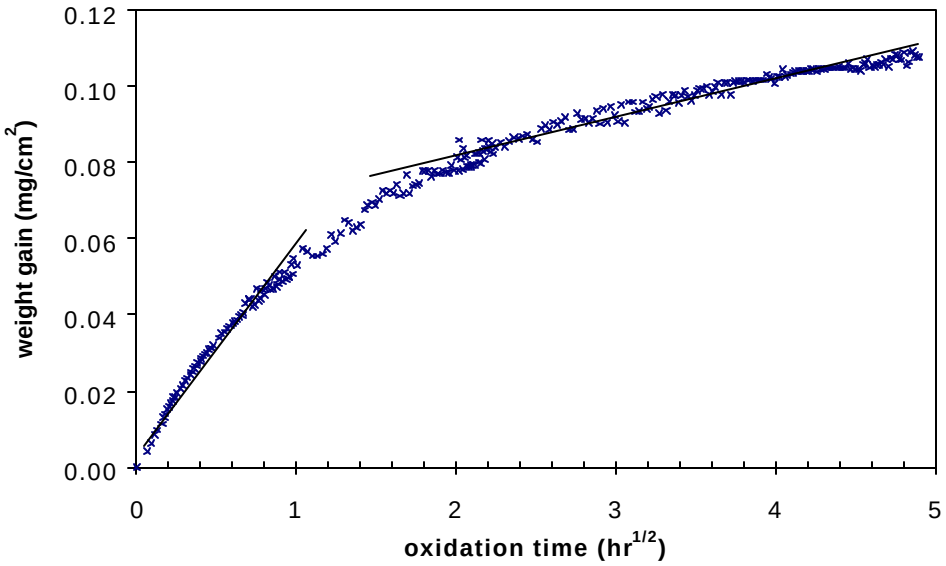

Figure 1: Oxidation kinetics Fe-40at%Al at 1000°C in oxygen.

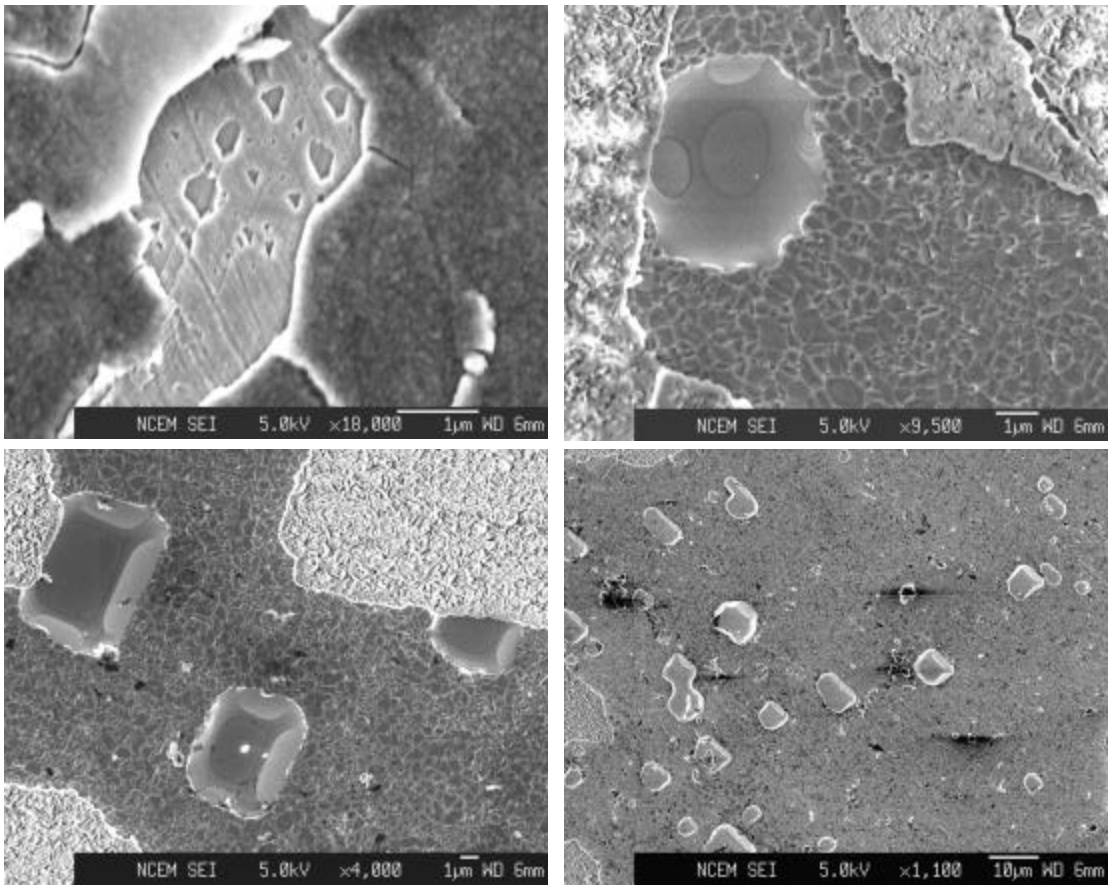

Figure 2: Morphology of interfacial pores and Al_2O_3 scales formed on Fe-40Al at 1000°C after 3 min (a), 1 hr (b) and 5 hr (c, d) oxidation. (d) Shows an example of pore coalescence.

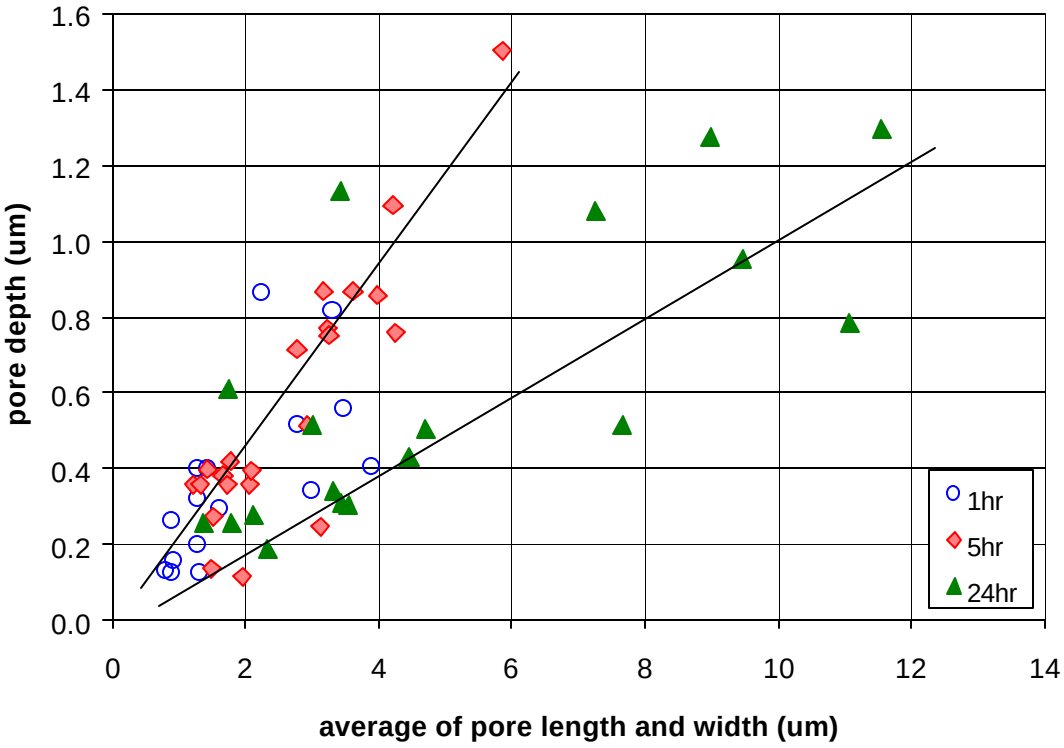

Figure 3: Relationship between pore depth and the average of pore length and width determined from AFM analyses.

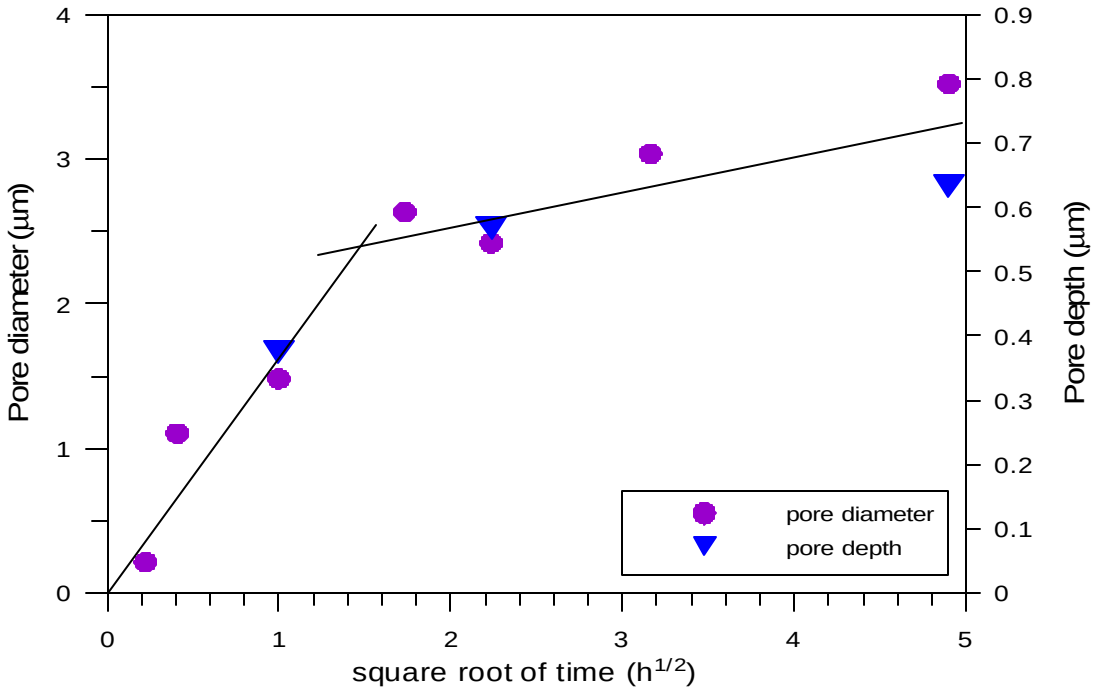

Figure 4: Change of average pore size (determined from SEM) and depth (determined from AFM) with the square root of time

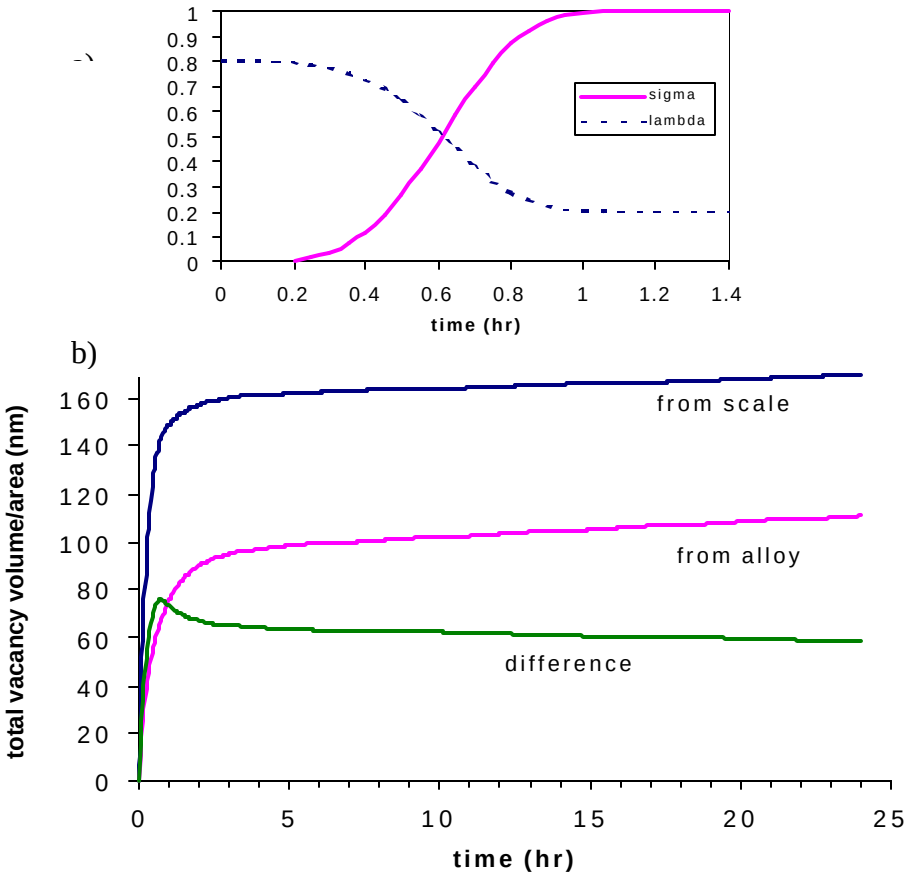

Figure 5: (a) Assumed time dependence of σ (the amount of α-Al_2O_3 in the scale) and λ (the fraction of scale growth by cation vacancy transport). (b) Calculated total amount of vacancies due to oxide growth and uneven diffusion in the alloy, and their difference.

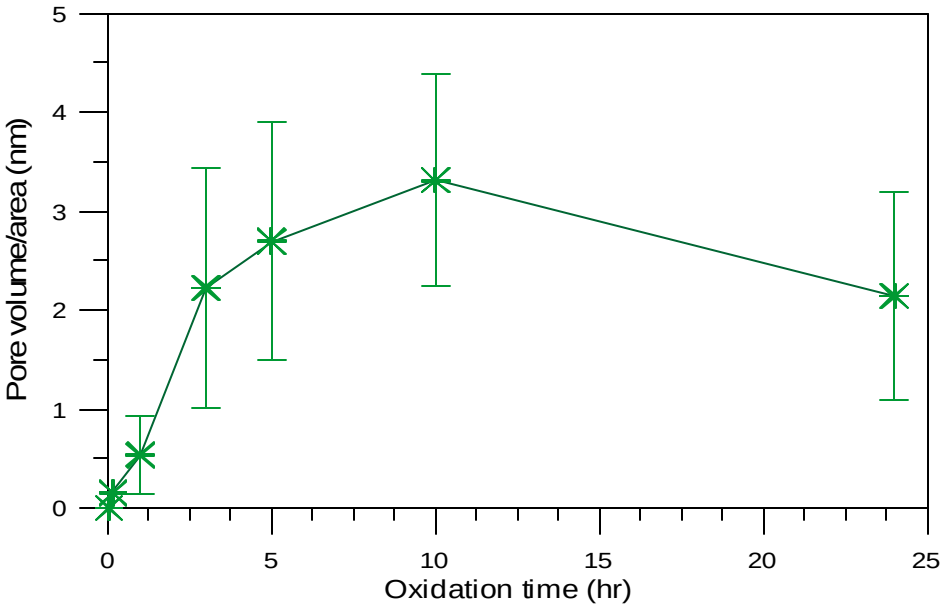

Figure 6: Experimentally determined total pore volume as a function of oxidation time.